Biomass-derived activated carbon as catalyst in the leaching of metals from a copper sulfide concentrate

A. Méndez [a,*], M.L. Álvarez [a], J.M. Fidalgo [a], C. Di Stasi [b], J.J. Manyà [b], G. Gascó [c]

[a] *Mining and Geological Engineering Department, Mining and Energy School, Universidad Politécnica de Madrid, Madrid, Spain*
[b] *Aragón Institute of Engineering Research (I3A), Thermochemical Processes Group, University of Zaragoza, Escuela Politécnica Superior, Spain*
[c] *Agricultural Production Department. School of Agriculture, Food and Biosystems Engineering, Universidad Politécnica de Madrid, Spain*

ARTICLE INFO

ABSTRACT

Chalcopyrite is the resource with the highest amount of Cu content representing around 70–80% of the known reserves in the world. However, chalcopyrite like other copper sulfides, is usually found in deposits with grades around 0.4–0.5% copper. The exploitation of these reserves using traditional flotation methods followed by pyrometallurgical treatment of copper concentrate is at the limit of economic viability. Hydrometallurgical route would be more suitable for treating of these low-graded sulfide ores. However, chalcopyrite is refractory in ferric/sulfuric acid media and shows slow dissolution rates. For this a number of researches were carried out to accelerate the kinetics of leaching by adding pyrite, iron powder, nanosized silica, coal and activated carbon. The main objective of the present work was to study the use of one biomass-derived activated carbon as catalysts in the leaching of copper from chalcopyrite. Sulfuric acid solution of pH 1 with 5 g L^{-1} of Fe^{3+} was used as leaching agent. Experiments were performed at 90 °C and 250 rpm, during 48 and 96 h. Concentration of Cu, Zn, As, Sb and Co in the liquid phase was determined in order to evaluate their extraction degree, whereas solid residues were characterized by SEM-EDS and XRD. The presence of biomass-derived activated carbon significantly increased the extraction of copper, decreasing the leaching of arsenic. Furthermore, the use of biomass-derived activated carbon led to lower amounts of crystalline sulfur in the final residue.

1. Introduction

Metals are crucial for word society, economy and industry. By global production volume, copper is the third metal after iron and aluminium. It was been widely used in electrical, electronic and communications applications. Nowadays, copper is also a strategic metal in emerging technologies such as wind generators, solar photovoltaics or electric vehicles that could drive copper demand in the coming years (Ciacci et al., 2020). Demand and price of copper are increasing in the last years leading to a general depletion of the world's high-grade mineral reserves. Chalcopyrite represents around 70–80% of the known copper reserves in the world (Norgate and Jahanshahi, 2010; Wang, 2005) and like other copper sulfides, chalcopyrite is usually found in deposits with low-grades (0.4–0.5% copper). Many of these low-grade resources around the world are uneconomic due to the expense of the flotation and smelting or pressure oxidation required to extract copper (Barton and Hiskey, 2022). Nevertheless, hydrometallurgical route is limited due to

chalcopyrite refractoriness in traditional ferric/acid media showing slow dissolution rates and consequently, low copper extraction. Córdoba et al. (2008) achieved <3% of copper extraction after 13 days of leaching with ferric ion at 35 °C. The copper extraction increases with temperature but were necessary more than 7 days of leaching to recover 80% of copper. Traditionally, low leaching rate is attributed to the formation, on the chalcopyrite surface, of passive layers composed of elemental sulfur (Dutrizac, 1989; Majima et al., 1985; McMillan et al., 1982), copper-rich polysulfides (Ammou-Chokroum et al., 1977; Hackl et al., 1995), or different ferrous and ferric salts (Córdoba et al., 2008). These coating layers have extremely low electrical conductivities and could hinder the transfer of electrons and ions to the chalcopyrite core leading to a limited extent of copper dissolution (Koleini et al., 2011; Watling, 2013).

During the last years, the use of several species as a means of improving the kinetics of chalcopyrite leaching was investigated (Barton and Hiskey, 2022). Most of these novel lixiviants require relatively high

temperatures, high oxidant concentrations, and/or fine grain sizes to leach chalcopyrite compared to traditional ferric acid method (Barton and Hiskey, 2022).In order to accelerate the kinetics of chalcopyrite leaching in ferric acid medium, several catalysts have been added such as pyrite (Koleini et al., 2011; Mehta and Murr, 1983), manganese dioxide (Gantayat et al., 2000; Nakazawa et al., 2016), nanosized silica (Misra and Fuerstenau, 2005), and more recently, carbon powder or activated carbon (Álvarez et al., 2021; Ma et al., 2017; Nakazawa et al., 2016; Okamoto et al., 2004). All of themhave proved to increase the copper dissolution rates. Nakazawa (2018) suggested that the enhanced kinetics of chalcopyrite leaching in the presence of carbon black could be ascribed to a decrease in the redox potential, as well as to galvanic interaction that takes place between chalcopyrite and carbon matrix. Álvarez et al. (2021) recently observed that the addition of four different carbon materials reduced the redox potential and the pH of leaching systems (copper and zinc from a complex mineral sulfide concentrate) resulting in possible changes in reaction mechanisms. This effect was quantitatively different depending on the characteristics and the amount of carbon material added.

It is well known that carbon materials can donate, accept, or transfer electrons from or to their surrounding environments. The ability of a given carbon material to reduce (or oxidize) its environment strongly depends on the nature of the functional groups available into the carbon matrix. In this sense, the electron-donating moieties (i.e., reducers) from carbons could be phenolic species, whereas quinones and poly-condensed aromatic structures might represent the electron-accepting moieties and act as oxidants (Klüpfel et al., 2014). In addition to the charging and discharging cycles of surface functional groups, direct electron transfer through carbon matrices might also explain the improvement in the electron transfer rate across the interface of carbon material and the external donors and acceptors (Sun et al., 2017). Hence, it is expected that carbon materials having an appropriate electronic conductivity and porosity development, such as designed activated carbons, could facilitate the reachability of the redox active sites by dissolved exogenous compounds (Yuan et al., 2017).

Carbon can be found in a wide variety of allotropes, from crystalline (diamond and graphite) to amorphous (carbon black, charcoal, biochar or activated carbon). In the past decade, the nanostructured forms of crystalline carbon (fullerenes, carbon nanotubes and graphene) have received the most attention due to remarkable and unusual physico-chemical properties. However, the main disadvantage of using these crystalline nanocarbons for environmental or catalysts application is their high production costs. Alternatively, carbon materials derived from renewable resources, such as lignocellulosic biomass or organic wastes, might play a very powerful role not only to replace fossil-based materials, but also to boost sustainable bio-economy. Slow pyrolysis is the most common route to produce biomass-derived carbons. Despite the fact that the resulting biochar (or charcoal) has poor surface functionality (only some C—O, C=O and OH groups can be present) and limited surface area (mainly composed of narrow micropores), its porosity and surface chemistry can be relatively easily tuned for a given application, resulting in a very promising platform to synthesise valuable and tailor-made functional materials. In the last years, special attention has been focused on developing biochar-derived materials to be used as electrode materials in energy storage devices, including Li-ion batteries, Li-S batteries, Na-ion batteries, and supercapacitors (Li et al., 2021; Panahi et al., 2020). Despite the fact that each electrochemical application brings its own requirements, the current state of knowledge reveals that developing biomass-derived activated carbons with well-developed hierarchical porous structure (i.e., containing micro, meso and macropores) seem to be highly appropriated (Kang et al., 2018). Activated carbons having a hierarchical porosity can be produced from the raw biochar through either physical or chemical activation. During the physical activation process, biochar is partially gasified (with CO_2, steam or other oxidizing agents) at temperatures ranging from 800 to 900 °C. Physical activation usually leads to carbons having a well-developed microporosity with a certain contribution from meso-porosity (Liu et al., 2015) showing low environmental impact that chemical activation processes.

The main objective of the present work is to analyse the potential application of a biomass-derived physically activated carbon as catalysts in the leaching of copper from a copper sulfide concentrate rich in chalcopyrite. Leaching experiments were performed at two different reaction times (48 h and 96 h). Extractions of Cu, Zn, As, Sb and Co were determined taking account the concentration of Cu, Zn, As, Sb and Co in the liquid (leaching and washing) solutions, whereas solid residues were characterized by scanning electron microscopy coupled with energy-dispersive X-ray spectroscopy (SEM-EDS) and X-ray diffraction (XRD) in order to elucidate the catalytic effect of carbon material.

2. Materials and methods

2.1. Materials selection and characterization

One concentrate rich in chalcopyrite (S1) was selected from the massive sulfide deposit of the Iberian Pyrite Belt located in the south-west of Spain.S1 was collected after grinding and flotation processes (80% < 50 μm). Then, sample was air-dried, crushed and sieved below 50 μm using an agate mortar. Wavelength X-ray fluorescence (WDXRF) was performed in an ARL ADVANT'XP + sequential model from THERMO (SCAI-Malaga University). Concentration data were obtained using the UNIQUANT Integrated Software. XRD was performed using a Bruker diffractometer model D8 Advance A25.

Biomass-derived activated carbon (BJ1) was obtained by pyrolysis of wheat straw pellets and subsequent pressurized physical activation with CO_2 as follows: pristine biochar was produced by pyrolysis of binder-free wheat straw pellets in a fixed bed reactor at atmospheric pressure. 400 g of biomass was placed inside the reactor and heated up to 500 °C at an average heating rate of 5 °C min^{-1} under a nitrogen atmosphere (further details on the pyrolysis device and procedure can be found in Greco et al, 2018). The resulting biochar, which was previously ground and sieved to a size range of 0.212–1.41 mm, was then physically activated with CO_2 at 700 °C and an absolute pressure of 1.0 MPa using a fixed-bed reactor (made of nickel–chromium alloy UNS N06600; 28 mm ID and 600 mm height). Biochar was initially heated under pure N_2 at a heating rate of 10C min^{-1} until the target temperature (i.e., 700 °C) was reached. Then, the gas inlet was switched from N_2 to CO_2 for a run time of 2.5 h. The gas hourly space velocity (GHSV) was kept constant at 3500 h^{-1} (Di Stasi et al, 2021).

Produced BJ1 was characterized in terms of pH, redox potential (Eh), BET specific surface area, ash content and elemental analysis (C, H, N, O and S). pH and Eh were measured in aqueous solutions (4 g·L^{-1}) using two meters from Crison (micro pH 2000 and pH 60 DHS equipment for pH and Eh, respectively). C, H, N and S contents were determined by dry combustion using a LECO CHNS 932 analyzer (SCAI-Malaga University). Ash content was measured by combustion of sample at 850 °C during 24 h in an electrical mufle furnace. Oxygen was obtained by difference as 100%–(%C+%H+%N+%S+%Ash). Textural parameters of BJ1 were determined from the N_2 adsorption isotherm which was acquired using an ASAP 2420 gas sorption analyser from Micromeritics (SCAI-Málaga University). Sample (around 120 mg) were previously degassed under dynamic vacuum conditions to constant weight at 150 °C. The apparent specific surface area (S_{BET}) and micropore volume (S_{mic}) were estimated using the MicroActive software (v-4.03) from Micromeritics.

Finally, BJ1 was analysed by Fourier transform infrared spectroscopy (FTIR) using a bruker vertex70 FT-IR spectrophotometer (SCAI-Malaga University). The measurements were carried out by transmission with the sample dispersed in a KBr. For the acquisition of the spectra, a standard spectral resolution of 4 cm^{-1}in the spectral range of 4000–400 cm^{-1} as well as 64 accumulations per sample. The target used has been the air.

Table 1
Contents (in wt. %) of main elements and mineralogical components in copper sulfide concentrate (S1 sample).

Sample	Cu (%)	Fe (%)	S (%)	Zn (%)	Si (%)	Al (%)	Mg (%)	Sb (%)	As (%)	Clp* (%)	Py** (%)	Sph*** (%)
S1	17.61	20.68	13.36	6.76	1.67	0.664	0.413	0.229	0.123	52.6	8.4	32.2

*Chalcopyrite; **Pyrite; ***Sphalerite.

2.2. Leaching experiments

A thermostatic bath with stirring GFL 1083 (heating power of 1500 W at 230 V) was used for the leaching tests which were carried out at 90 °C and 250 rpm in 250 mL ISO borosilicate glass jars using H_2SO_4 solutions (at pH 1) with a concentration of $5gL^{-1}$ of Fe (III). The temperature (90 °C) and stirring speed (250 rpm) were controlled during the leaching process until 48 and 96 h. Eh of the leaching agent solution was 547 mV. The purity of Sigma-Aldrich® sulfuric acid and Fe (III) sulfate hydrated Labkem was 97% and 99.5%, respectively. In each experiment, 2.5 g of S1 was weighed in the borosilicate glass jar. Except for the control, the ratios S1/BJ1 (weight/weight) were 1/0.5 and 1/0.25. Then, 50 mL of leaching agent was added. Two leaching experiments were performed for each S1/carbon material mixture using two reaction times: a first one until 48 h and a second one until 96 h. During leaching experiment, jars were opened every 24 h, in order to ensure adequate oxygenation of the leaching system. At the end of the reaction (48 h and 96 h) the pulp was filtered and washed two times with 50 mL of H_2SO_4 solution at pH 2 to recover metals adsorbed on carbon surface. Contents of Cu, Zn, As, Co and Sb in both, the leaching and washed solutions, were determined by ICP-MS (SCIEX Perkin Elmer) from SCAI-Malaga University. The total metal extraction degree (%) was determined considering the content of Cu, Zn, As, Co and Sb in the leaching and washed solutions and their initial content in the S1 sample.

The final solid residues obtained after leaching during 48 h and 96 h were ground to a fine powder, for which the agate mortar was used and analyzed by XRD using a Bruker diffractometer, model D8 Advance A25 (SCAI-Malaga University), measuring in transmission with the sample located between two sheets and the equipment consists of an automatic sample loader and a rotating sample holder. In the path of the incident beam, the optical system of this equipment has a primary monochromator that makes the radiation reaching the sample monochromatic. The detection system is a LYNXeye XE, with the maximum active length. Measurements were made from 3° to 40° (2θ) for 4 h. To carry out the measurement, a Mo diffractometer was used to avoid the noise caused by the Fe-containing phases in conventional Cu-tube equipment. Crystalline phases were identified using PANalytical's High Score Plus software. Quantitative XRD results were obtained through the Rietveld refinement method.

In addition, SEM-EDS analysis was performed using a Helios Nanolab 650 dual beam microscope from FEI Company, fitted with a Schottky field emission source for SEM (FESEM) and a Tomohawk focused ion beam (FIB). The microscope is equipped with energy dispersive X-ray (EDS) and electron-backscatter diffraction (EBSD) detectors from Oxford Company.

3. Results and discussion

3.1. Characterization of feedstocks

Table 1 shows the contents of the main elements and mineralogical components of S1. XRD data referred to crystalline components was quantified by Rietveld refinement method. The main crystalline

component was chalcopyrite (52.6 wt%), followed by sphalerite (32.2 wt%) and pyrite (8.5 wt%). According to this composition, the most abundant metal was iron (20.68 wt%), followed by copper (17.61 wt%) and zinc (6.76 wt%). It is important to highlight the relative high content of arsenic (0.123 wt%) and antimony (0.229 wt%).

With respect to the biomass-derived activated carbon (BJ1), its physicochemical properties are summarized in Table 2. The relatively low C and high as contents in BJ1 can be explained by the extent of the Boudouard reaction during the activation process (Di Stasi et al., 2021). In addition to the aromatic character of the carbon network (H/C ratio of 0.10 as shown in Table 2), the high ash content in BJ1, also contributed to the increase in its pH, which was alkaline (10.97). With regards to Eh, BJ1 exhibited a relatively low value (217 mV).

Concerning the textural properties, BJ1 showed a relatively high S_{BET} value of 676 m^2 g^{-1}, due to high microporosity developed during pyrolysis and to a much greater extend during activation with CO_2 (Di Stasi et al., 2021). It is known that pore size distribution and specific surface area play an important role in the adsorption capacity of carbon materials, but also in the redox properties and consequently in their catalytic activity (Li et al., 2020). Fig. 1 provides the N_2 adsorption–desorption isotherm of BJ1 that was hybrid-shaped and belong to type II-IV, according to the IUPAC classification (Thommes et al., 2015). The adsorption of N_2 at low relative pressure (P/P0 < 0.1) was related to the presence of microporosity and it reflects a greater development of porosity in BJ1 due to activation with CO_2. Additionally, BJ1 showed a hysteresis loop providing further evidence for the existence of some capillary condensation.

Previous research studies reported that the presence of functional groups determined the catalytic activity of carbon materials for oxidative leaching purposes of sulfide minerals (Jahromi and Ghahreman, 2019). Indeed, some oxygen functional groups such as hydroxiquinones and quinones, can promote reversible redox reactions (Jahromi and Ghahreman, 2019). As mentioned above, the low atomic H/C ratio of BJ1 indicates high aromaticity development. Hammes et al. (2006) indicated that materials with highly condensed carbon aromatic rings typically have atomic H/C ratios lower than 0.3, such as was the case of BJ1. On the other hand, both the oxygen content (12.26 wt%) and the atomic O/C ratio of BJ1 are relatively high, suggesting a certain availability of oxygen-containing groups (e.g. carboxyl, hydroxyl, carbonyl and/or ester groups). This fact could be explained by the relatively low temperature used during physical activation (700 °C). Not only concentration, type and distribution of functional groups on the carbon surface, but also oxygen availability, and pre-treatment can change the catalytic properties of carbon materials. In order to broaden the characterization of the oxygenated functional groups, FTIR analysis (see Fig. 2) was carried out. The broad band at 3400 cm^{-1} was attributed to OH stretching vibration in carboxyl and hydroxyl groups. The small peaks at 2900 and 2850 cm^{-1} indicated that BJ1 had low content of aliphatic structures according to its low atomic H/C ratio (see Table 2). The peak at 1620 cm^{-1} could be attributed to C=O vibrations in quinones and conjugated ketones, whereas the band at 1450 cm^{-1} can be related to C=C stretching in aromatic structures. The small peak at 870 cm^{-1} was associated to C–H aromatic groups. With respect to the small
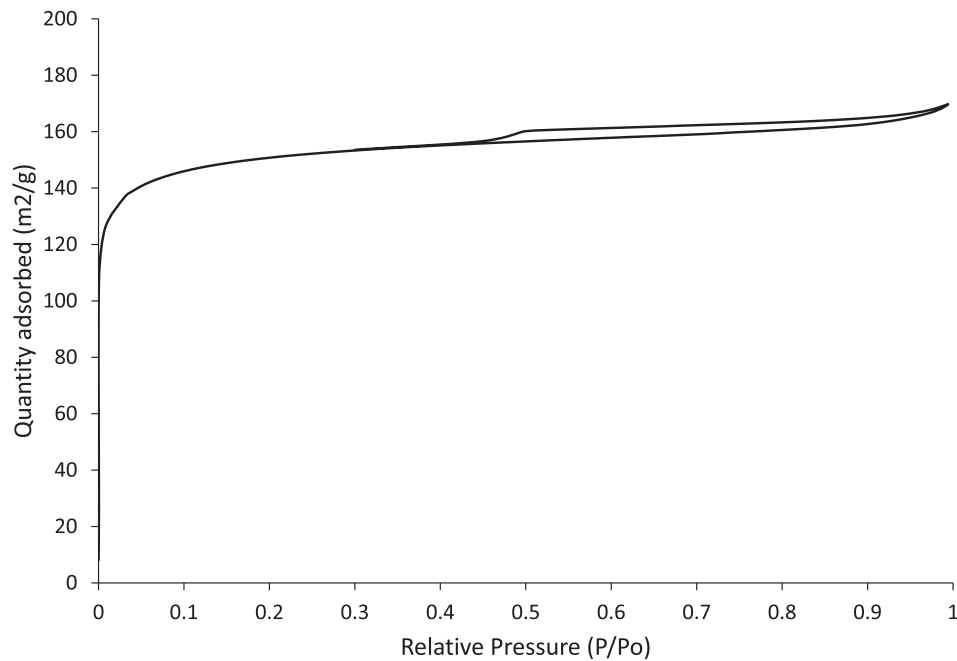
Table 2
Properties of biomass-derived activated carbon (BJ1).

Sample	C (%)	H (%)	N (%)	S (%)	O (%)	H/C	O/C	N/C	S_{BET} (m^2/g)	S_{mic} (m^2/g)	pH	Eh (mV)	Ash (%)
BJ1	51.74	0.06	1.22	0.00	12.26	0.10	0.18	0.08	676	646	10.97	217	34.21

Fig. 1. N$_2$ adsorption–desorption isotherms of biomass-derived activated carbon (BJ1).

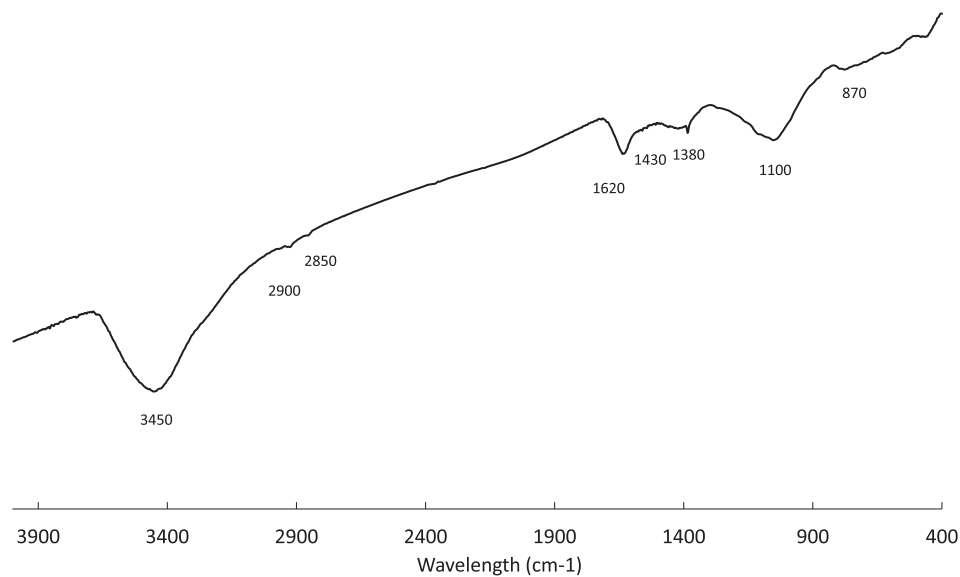**Fig. 2.** FTIR spectra of biomass-derived activated carbon (BJ1).

peak at 1380 cm^{-1}, it could be attributed to N-containing groups. Finally, the broad band between 1000 and 1300 cm^{-1} is related to the presence of aliphatic ethers (C—O—C) and alcohols (C—O) stretching. Results from FTIR spectrum show good agreement with those previously reported by Di Stasi et al., (2021). It is know that during the activation reaction, carbon dioxide would dynamically change the structure of biochar by introducing of multiple active sites, including oxygen-containing functional groups. In summary, FTIR spectrum of BJ1 revealed the presence of C—O—C and C—O bounds related to ethers and alcohols. These functional groups available in surface, coupled with the high aromatic carbon structure contribute to the reductant properties of BJ1 (i.e., low Eh value reported in Table 2).

3.2. Extraction of metals

Fig. 3 shows the extraction yields of Cu (3.a), Zn (3.b), As (3.c), Sb (3. d) and Co (3.e). In the case of copper extraction, after 48 h, the addition of BJ1 in the ratio 1/0.25 increased the amount of copper extracted (compared to control condition) whereas its addition in the ratio 1/0.5 led to a slight decrease in the amount of Cu extracted. After 96 h of leaching, the catalytic effect of BJ1 was more pronounced, achieving highest extraction yield of 80 wt% when BJ1 was added at a ratio of 1/0.25. Previous published research studies reported that copper extraction was mainly controlled by the redox potential of the leaching solution (Tian et al., 2021), which is closely related to the Fe^{3+}/Fe^{2+} concentration ratio, and that it was enhanced at low redox potential
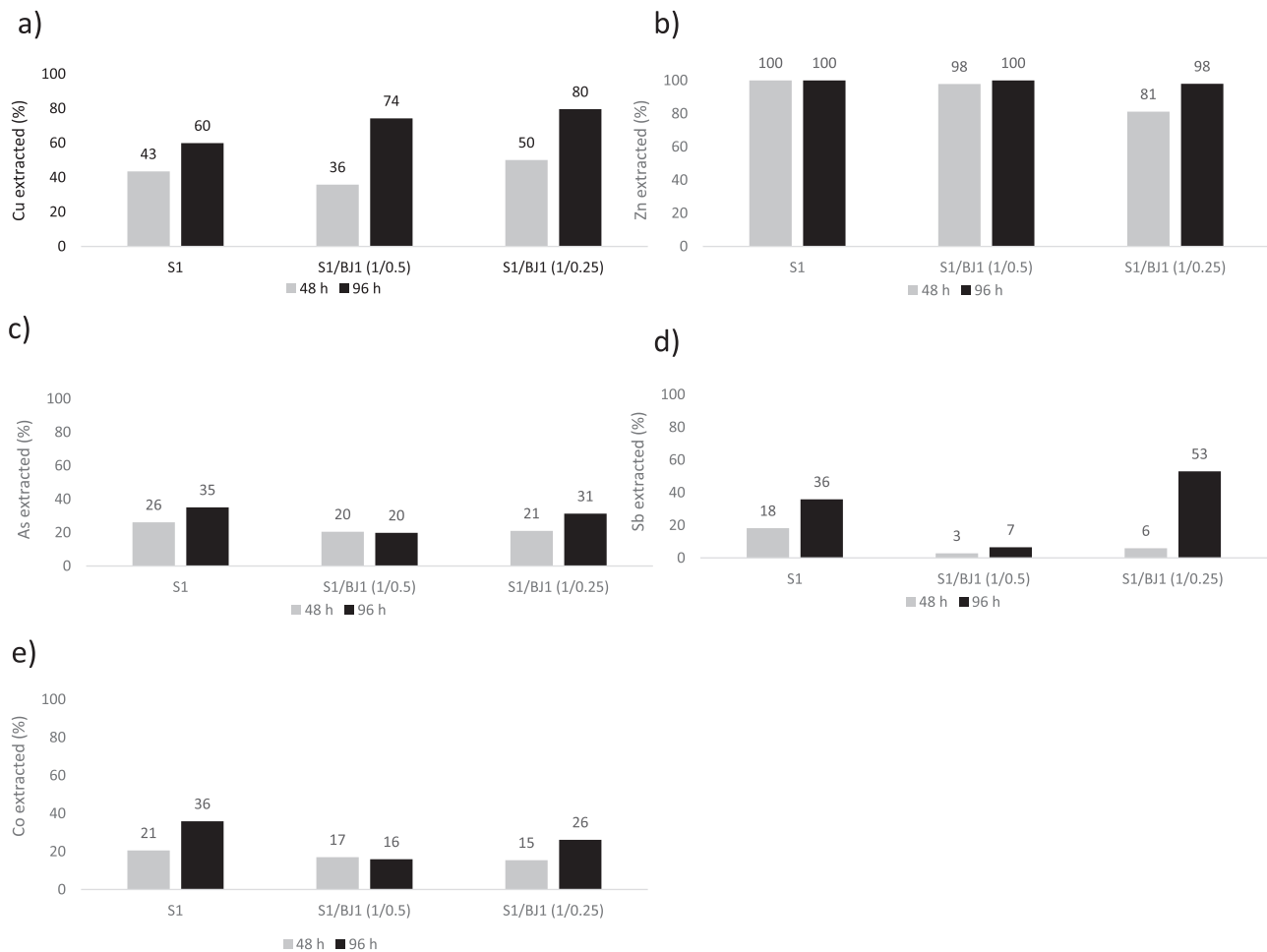
a)

b)

c)

d)

e)

Fig. 3. Total extraction of elements: a) Cu, b) Zn; c) As; d) Sb and d) Co.

Table 3
Eh (mV) of leaching solutions.

SAMPLES	Eh (mV)		
	0 h	48 h	96 h
S1	602	426	491
S1/BJ1 (1/0.5)	590	432	451
S1/BJ1 (1/0.25)	598	420	434

values due to the formation of intermediate species that were then easily oxidized (Hiroyoshi et al., 2000). Nakazawa (2018) used carbon black in sulfuric acid media at 50 °C and suggested that the enhanced kinetics of chalcopyrite leaching could be attributed to (1) dissolution reactions at relatively low redox potentials, and (2) galvanic interaction between chalcopyrite and carbon black. This author observed that the enhancement of chalcopyrite leaching did not occur without direct contact between chalcopyrite and carbon black. Furthermore, the addition of carbon black decreased the Fe^{3+}/Fe^{2+} concentration ratio in the early stages of leaching and dropped the redox potential below 600 mV. Other researchers (Córdoba et al., 2008; Hiroyoshi et al. 2000) concluded that the redox potential appears as key factor in determining the leaching of chalcopyrite and proposed a critical potential below which chalcopyrite can dissolve through the formation of intermediate species. Table 3 shows that, with the exception of sample S1/BJ1 1/0.5 at 48 h, the redox potential of the leaching system was lower in the presence of BJ1. The fact that the highest Cu extraction yields were obtained when BJ1 was added at its lowest mass ratio (1/0.25) could be explained by the extent of certain electrochemical interactions between catalyst and sulfide

minerals. In this sense, when more activated biochar was added to the leaching solution, the measured Eh after 48 and 96 h was higher than that measured when BJ1 was added at the ratio of 1/0.25 due to the greater extent of the above-mentioned interactions. In addition, the possible modification of the surface properties of the carbon material-when it immersed in the leaching solution (Jahromi and Ghahreman, 2019) can also partly explain the different catalytic effects observed for the two tested S1/BJ1 mass ratios.

The higher extraction yields for Zn (Fig. 3.b) were related to the higher leaching rates of sphalerite (Álvarez et al., 2021). 100 wt% of Zn was extracted after 48 h of S1 leaching. In this case, the addition of BJ1 decreased the kinetics of zinc leaching; however, after 96 h of leaching, it was also possible to reach high Zn extraction yields (98 wt% for S1/BJ1 at the ratio 1/0.25; for which a highest Cu extraction yield of 80 wt% was attained).

Fig. 3.c shows the As extraction yields which slightly decreased with the addition of BJ1. A low leaching rate of As represents an important improvement in the hydrometallurgical recovery of metals from sulfides concentrates, since As could be immobilized in the residue. In addition, the low As concentration in the leaching solution reduces costs of purification before electrowinning. Jahromi and Ghahreman (2018) studied the arsenic precipitation during carbon catalyzed leaching of enargite (Cu_3AsS_4) and found that arsenic precipitated as scorodite ($FeAsO_4 \cdot H_2O$). They also found that it was necessary to have high ferric content (5 g L^{-1}) in the leaching solution and high carbon ratios. In the present study, were the As content was 0.123 wt% (Table 1), the XRD pattern of S1 does not reveal the presence of any arsenic crystalline specie. Hence, the addition of activated carbon to the leaching system

Table 4
XRD analysis of solid residues after leaching process during 48 and 96 h.

Sample	Chalcopyrite	Pyrite	Sphalerite	Cristobalite	Sulfur
S1 48 h	49.5	35.1	<1	2.3	12
S1 96 h	40.0	35.4	<1	2.6	21.0
S1/BJ1 1/0.25 48 h	44.3	40.2	5.0	7.4	2.4
S1/BJ1 1/0.25 96 h	31.3	45.4	3.1	6.6	12.4

resulted in an inhibition of As leaching, which was particularly marked at the S1/BJ1 mass ratio of 1/0.5. Regarding the behaviour of Sb leaching (see Fig. 3.d), the addition of BJ1 at the lower mass ratio (1/0.25) led to an increase in the amount of Sb extracted (53 wt%). However, using a larger amount of carbon (i.e., mass ratio of 1/0.5) resulted in a very low Sb extraction yield of only 7 wt% after 96 h.

Finally, leaching rate of Co, which was modest under to control condition (36 wt% after 96 h) was further decreased to 26 and 16 wt% (after 96 h) when BJ1 was added at S1/BJ1 mass ratios of 1/0.25 and 1/0.5, respectively (see Fig. 3.e).

In summary, it can be concluded that the addition of BJ1 resulted in an improvement in the leaching of Cu without significantly affecting the Zn extraction yield. Interestingly, BJ1 also inhibited the extraction od As and Sb.

3.3. Characterization of solid residues obtained after leaching experiments

Solid samples obtained after leaching (samples S1 and S1/BJ1 1/0.25) at 48 and 96 h were selected for subsequent characterization. Table 4 reports the main crystalline mineralogical species and their proportion (wt. %) in the final residue. The new specie formed is sulfur due to oxidation of sulfide sulfur to elemental sulfur. It is important to note the high difference between sulfur content in the leaching residue with BJ1 and without carbon addition. SEM-EDS micrographs of the leaching residue S1/BJ1 at 96 h shows that sulfur was adsorbed on the surface of BJ1 (Fig. 4). This phenomenon can play an important role in the leaching mechanism of chalcopyrite catalysed by activated carbons, inhibiting the formation of sulfur passivation layer on their surface and consequently, increasing the kinetics of the process. The adsorption of elemental sulfur by carbon materials can simplify the sulfur removal from the leaching residue, reducing the environmental impact of final mine wastes (Jahromi and Ghahreman; 2019).

Other mineralogical species found in the leaching residues were chalcopyrite, pyrite, sphalerite and quartz. The results shown in Table 4 suggest that, under the experimental conditions used in the present research, crystalline intermediate species were not formed in spite of the reduction in Eh (see Table 3). Hiroyoshi et al (2000) pointed out that the redox potential has to be low enough for Cu_2S formation, whereas jarosite precipitation was favoured at very high redox potentials (Córdoba et al., 2008).

Analysis of initial S1 sample (Fig. 5.a) and leaching residues (Fig. 5.b and 5.c) by SEM-EDS showed the presence of chalcopyrite (Points 1 and 3, Fig. 5.a), pyrite (Point 2, Fig. 5.a) and small particles of quartz (Point 4, Fig. 5.a) in the initial concentrate. After 48 h of leaching (Fig. 5.b), the solid reside showed the presence of chalcopyrite (1), with the surface altered by leaching, and pyrite (2–4). Analysis of residue obtained after 48 he of leaching of S1/BJ1 showed the presence of pyrite (Points 1 and 3, Fig. 5.c), carbon with adsorbed sulfur (Point 5, Fig. 5.c), and some particles of chalcopyrite greatly altered (Points 2 and 4) indicating the preferential leaching of Fe over Cu from chalcopyrite. These species do not appear in the solid residues obtained after 96 h of leaching. Fig. 6 shows SEM and SEM-EDS images at high resolution. These new structures originated at the surface of chalcopyrite in the presence of BJ1, show low Fe concentration and consequently Cu enrichment that do not appear in the DRX probably due to the high alteration of the crystalline
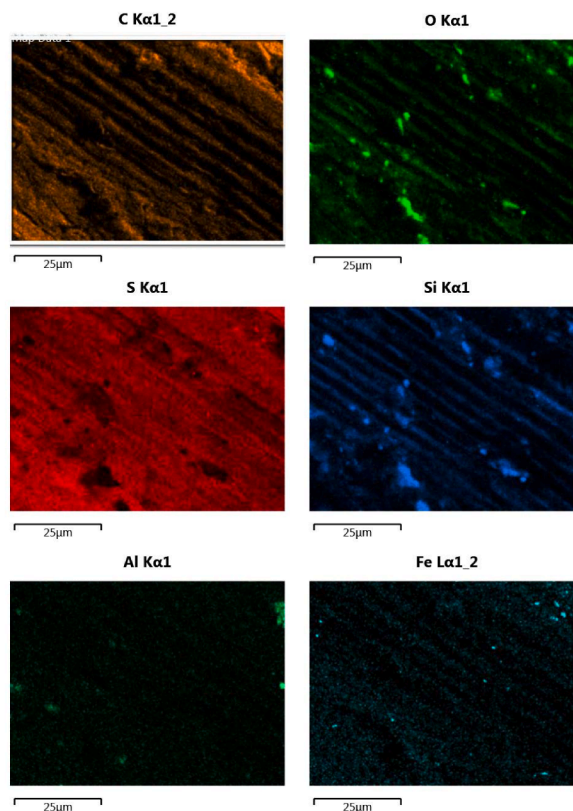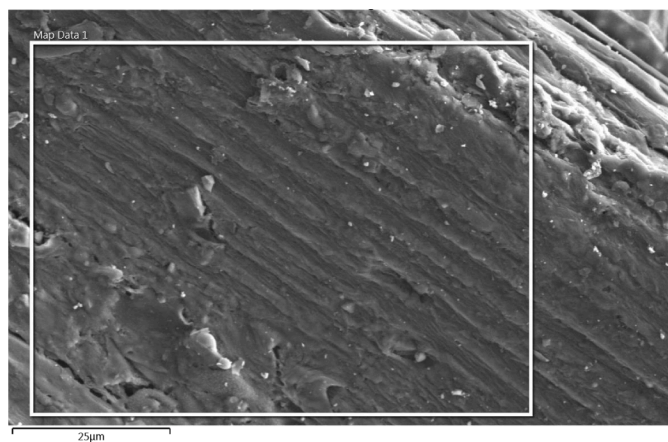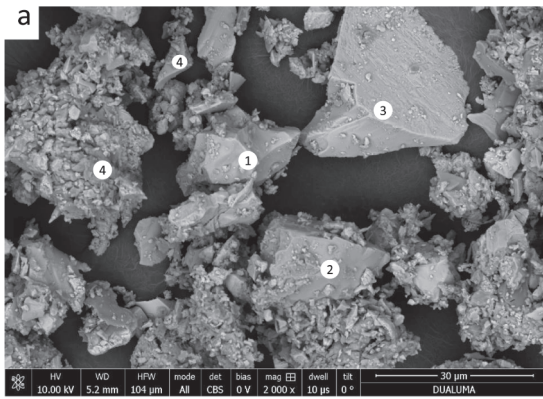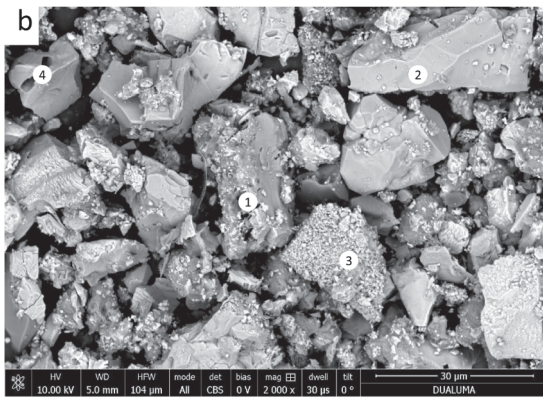
S1-BJ1-96h

Fig. 4. SEM-EDS images of S1/BJ1 residue after 96 h of leaching.

a — RT

Point	Weight content (%)					
	S	Fe	Cu	O	Si	Al
1	28.29	30.45	41.25			
2	46.67	53.33				
3	26.75	34.01	37.79	1.45		
4	2.87	31.02		44.25	8.63	9.00

SEM-EDS of S1/BJ1 at 48 h

b — RT-48h

Point	Weight content (%)					
	S	Fe	Cu	O	Si	Al
1	36.41	30.45	32.49		0.66	
2	47.52	52.44				
3	38.49	61.51				
4	47.83	51.84				

c
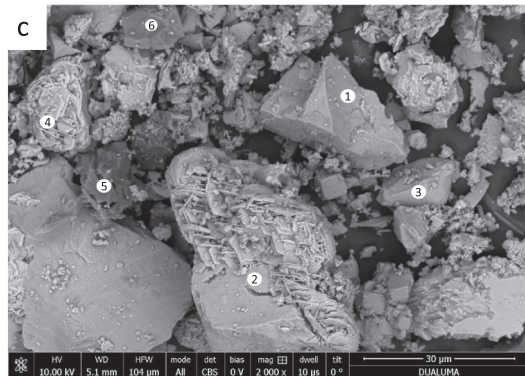
Point	Weight content (%)						
	S	Fe	Cu	O	As	C	Si
1	47.89	52.11					
2	35.02	34.35	30.63				
3	47.47	51.36			1.17		
4	35.98	5.64	44.53	6.17			3.50
5	25.26	1.19		5.72		66.94	
6	3.97	2.86		40.26			52.91

d
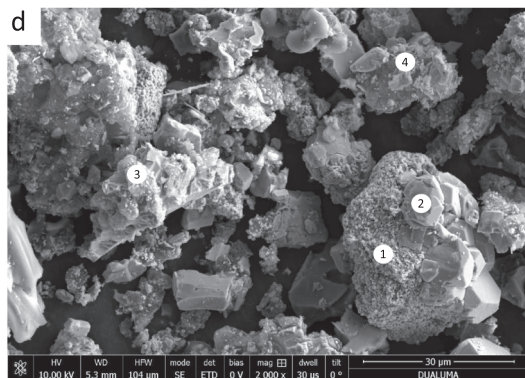
Point	Weight content (%)						
	S	Fe	Cu	O	As	C	Si
1	43.07	50.54	2.36	2.88			1.16
2	47.93	52.05			0.52		
3	31.11	35.25	18.29	5.13			2.92
4	28.39	52.35	5.15	3.46		7.23	3.00
5							
6							

Fig. 5. SEM-EDS images of S1 (a) and leaching residues: S1 at 48 h (b); S1/BJ1 at 48 h (c); S1/BJ1 at 96 h (d).
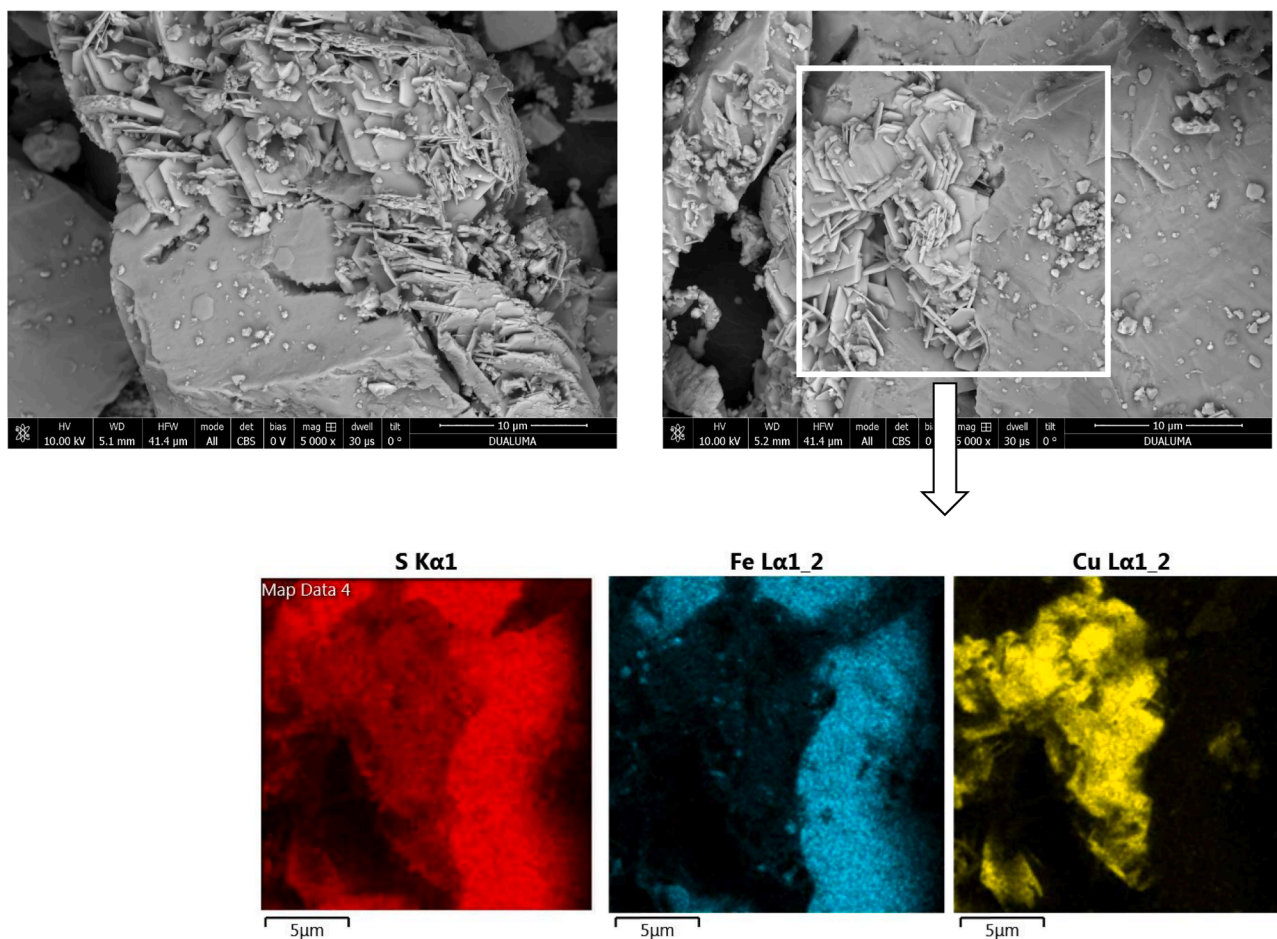
Fig. 6. SEM-EDS image of S1/BJ1 residue after 48 h of leaching.

structure. Finally, it is interesting to note the presence of arsenic join to pyrite particles (Point 3, Fig. 5.c and Point 2, Fig. 5.d) probably due to the high adsorption arsenic capacity of pyrite (Bulut et al., 2014).

4. Conclusions

From the findings presented above, the following main conclusions can be drawn:

1. Addition of biomass-derived activated carbon, a low-cost carbon material obtained by pyrolysis of biomass and subsequent CO_2 activation at mild temperature under moderate pressure, to Fe^{3+}/sulfuric leaching solution significantly increased the extraction rate of copper from chalcopyrite. The extraction of copper without carbon addition was 60% after 96 h of leaching at 90 °C and increase to 80% with the addition of biomass-derived activated carbon in the ratio 1/0.25.
2. Biomass-derived activated carbon inhibited the formation of sulfur crystals, probably due to the adsorption of intermediate sulfur species on their surface.
3. Biomass-derived activated carbon reduced the leaching of arsenic from copper sulfide concentrate. The extraction of arsenic without carbon was 35 % after 96 h of leaching and decreases to values of 31 or 20 % with the addition of biomass-derived activated carbon in the ratios of 1/0.25 and 1/0.5, respectively.
4. The use of biomass-derived activated carbon as catalyst in the leaching of chalcopyrite and sulfide concentrates can contribute to the development of sustainable hydrometallurgical processes.

Declaration of Competing Interest

The authors declare that they have no known competing financial interests or personal relationships that could have appeared to influence the work reported in this paper.

Acknowledgements

References

Álvarez, M.L., Fidalgo, J.M., Gascó, G., Méndez, A., 2021. Hydrometalurgical recovery of Cu and Zn from a complex sulfide mineral by Fe3+/H2SO4 leaching in the presence of carbon-based materials. Metals 11 (2), 286. https://doi.org/10.3390/met11020286.

Ammou-Chokroum, M., Cambazoglu, M., Steinmetz, D., 1977. Oxydation menagée de la chalcopyrite en solution acide: analyses cinétique de réactions. II. Modéles diffusionales. Bull. Soc. Fr. Minéral. Cristallogr. 100, 161–177.

Barton, I.F., Hiskey, J.B., 2022. Chalcopyrite leaching in novel lixiviants. Hydrometallurgy 207, 105775. https://doi.org/10.1016/j.hydromet.2021.105775.

Bulut, G., Yenial, U., Emiroglu, E., Sirkeci, A.A., 2014. Arsenic removal from aqueous solution using pyrite. J. Cleaner Prod. 84, 526–532. https://doi.org/10.1016/j.jclepro.2013.08.018.

Ciacci, L., Fishman, T., Elshkaki, A., Graedel, T.E., Vassura, I., Passarini, F., 2020. Exploring future copper demand, recycling and associated greenhouse gas emissions in the EU-28. Global Environ. Change 63, 102093. https://doi.org/10.1016/j.gloenvcha.2020.102093.

Córdoba, E.M., Muñoz, J.A., Blázquez, M.L., González, F., Ballester, A., 2008. Leaching of chalcopyrite with ferric ion. Part II: effect of redox potential. Hydrometallurgy 93 (3-4), 88–96. https://doi.org/10.1016/j.hydromet.2008.04.016.

Di Stasi, C., Greco, G., Canevesi, R.L.S., Izquierdo, M.T., Fierro, V., Celzard, A., González, B., Manyà, J.J., 2021. Influence of activation conditions on textural properties and performance of activated biochars for pyrolysis vapors upgrading. Fuel 289, 119759. https://doi.org/10.1016/j.fuel.2020.119759.

Dutrizac, J.E., 1989. Elemental sulphur formation during the ferric sulfate leaching of chalcopyrite. Can. Metall. Q. 28, 337–344. https://doi.org/10.1179/cmq.1989.28.4.337.

Gantayat, B.P., Rath, P.C., Paramguru, R.K., Rao, S.B., 2000. Galvanic interaction between chalcopyrite and manganese dioxide in sulfuric acid medium. Metall. Mater. Trans. B 31 (1), 55–61. https://doi.org/10.1007/s11663-000-0130-z.

Greco, G., Videgain, M., Di Stasi, C., González, B., Manyà, J.J., 2018. Evolution of the mass-loss rate during atmospheric and pressurized slow pyrolysis of wheat straw in a bench-scale reaction. J. Anal. Appl. Pyrol. 136, 18–26.

Hackl, R.P., Dreisinger, D.B., Peters, E., King, J.A., 1995. Passivation of chalcopyrite during oxidative leaching in sulfate media. Hydrometallurgy 39 (1-3), 25–48. https://doi.org/10.1016/0304-386X(95)00023-A.

Hammes, K., Smernik, R.J., Skjemstad, J.O., Herzog, A., Vogt, U.F., Schmidt, M.W.I., 2006. Synthesis and characterisation of laboratory charred grass straw (Oryza sativa) and chestnut wood (Castanea sativa) as reference materials for black carbon quantification. Org. Geochem. 37, 1629–1633. https://doi.org/10.1016/j.orggeochem.2006.07.003.

Hiroyoshi, N., Miki, H., Hirajima, T., Tsunekawa, M., 2000. A model for ferrous-promoted chalcopyrite leaching. Hydrometallurgy 57 (1), 31–38.

Jahromi, F.G., Ghahreman, A., 2019. Effects of surface modification with different acids on the functional groups of AFS catalyst and its catalytic effect on the atmospheric leaching of enargite. Colloids Interfaces 3 (2), 45. https://doi.org/10.3390/colloids3020045.

Jahromi, F.G., Ghahreman, A., 2018. In-situ oxidative arsenic precipitation as scorodite during carbon catalysed enargite leaching process. J. Hazard. Mater. 360, 631–638. https://doi.org/10.1016/j.jhazmat.2018.08.019.

Kang, X., Zhu, H., Wang, C., Sun, K., Yin, J., 2018. Biomass derived hierarchically porous and heteroatom-doped carbons for supercapacitors. J. Colloid Interface Sci. 509, 369–383. https://doi.org/10.1016/j.jcis.2017.09.013.

Koleini, S.M.J., Aghazadeh, V., Sandström, Å., 2011. Acidic sulphate leaching of chalcopyrite concentrates in presence of pyrite. Miner. Eng. 24 (5), 381–386. https://doi.org/10.1016/j.mineng.2010.11.008.

Klüpfel, L., Keiluweit, M., Kleber, M., Sander, M., 2014. Redox properties of plant biomass-derived black carbon (biochar). Environ. Sci. Technol. 48 (10), 5601–5611. https://doi.org/10.1021/es500906d.

Li, S., Shao, L., Zhang, H., He, P., Lü, F., 2020. Quantifying the contributions of surface area and redox-active moieties to electron exchange capacities of biochar. J. Hazard. Mater. 394, 122541. https://doi.org/10.1016/j.jhazmat.2020.122541.

Li, X., Zhang, J., Liu, B., Su, Z., 2021. A critical review on the application and recent developments of post-modified biochar in supercapacitors. J. Cleaner Prod. 310, 127428. https://doi.org/10.1016/j.jclepro.2021.127428.

Liu, W.-J., Jiang, H., Yu, H.-Q., 2015. Development of Biochar-Based Functional Materials: Toward a Sustainable Platform Carbon Material. Chem. Rev. 115 (22), 12251–12285. https://doi.org/10.1021/acs.chemrev.5b00195.

Ma, Y.-L., Liu, H.-C., Xia, J.-L., Nie, Z.-Y., Zhu, H.-R., Zhao, Y.-D., Ma, C.-Y., Zheng, L., Hong, C.-H., Wen, W., 2017. Relatedness between catalytic effect of activated carbon

and passivation phenomenon during chalcopyrite bioleaching by mixed thermophilic Archaea culture at 65 ∘C. Trans. Nonferr. Met. Soc. China 27 (6), 1374–1384. https://doi.org/10.1016/S1003-6326(17)60158-4.

Majima, H., Awakura, Y., Hirato, T., Tanaka, T., 1985. The leaching of chalcopyrite in ferric chloride and ferric sulfate solutions. Can. Metall. Q. 24 (4), 283–291. https://doi.org/10.1179/cmq.1985.24.4.283.

McMillan, R.S., MacKinnon, D.J., Dutrizac, J.E., 1982. Anodic dissolution of n-type and p- type chalcopyrite. J. Appl. Electrochem. 12 (6), 743–757. https://doi.org/10.1007/BF00617495.

Mehta, A.P., Murr, L.E., 1983. Fundamental studies of the contribution of galvanic interaction to acid-bacterial leaching of mixed metal sulfides. Hydrometallurgy 9 (3), 235–256. https://doi.org/10.1016/0304-386X(83)90025-7.

Misra, M., Fuerstenau, M.C., 2005. Chalcopyrite leaching at moderate temperature and ambient pressure in the presence of nanosize silica. Miner. Eng. 18 (3), 293–297. https://doi.org/10.1016/j.mineng.2004.06.014.

Nakazawa, H., Nakamura, S., Odashima, S., Hareyama, W., 2016. Effect of carbon black to facilitate galvanic leaching of copper from chalcopyrite in the presence of manganese (IV) oxide. Hydrometallurgy 163, 69–76. https://doi.org/10.1016/j.hydromet.2016.03.003.

Nakazawa, H., 2018. Effect of carbon black on chalcopyrite leaching in sulfuric acid media at 50 ∘C. Hydrometallurgy 177, 100–108. https://doi.org/10.1016/j.hydromet.2018.03.001.

Norgate, T., Jahanshahi, S., 2010. Low grade ores–smelt, leach or concentrate? Miner. Eng. 23 (2), 65–73. https://doi.org/10.1016/j.mineng.2009.10.002.

Okamoto, H., Nakayama, R., Kuroiwa, S., Hiroyoshi, N., Tsunekawa, M., 2004. Catalytic effect of activated carbon and coal on chalcopyrite leaching in sulfuric acid solutions. J. MMIJ 120 (10/11), 600–606. https://doi.org/10.2473/shigentosozai.120.600.

Panahi, H.K.S., Dehhaghi, M., Ok, Y.S., Nizami, A.-S., Khoshnevisan, B., Mussatto, S.I., Aghbashlo, M., Tabatabaei, M., Lam, S.S., 2020. A comprehensive review of engineered biochar: Production, characteristics, and environmental applications. J. Cleaner Prod. 270, 122462. https://doi.org/10.1016/j.jclepro.2020.122462.

Sun, T., Levin, B.D.A., Guzman, J.J.L., Enders, A., Muller, D.A., Angenent, L.T., Lehmann, J., 2017. Rapid electron transfer by the carbon matrix in natural pyrogenic carbon. Nat. Commun. 8 (1) https://doi.org/10.1038/ncomms14873.

Thommes, M., Kaneko, K., Neimark, A.V., Olivier, J.P., Rodriguez-Reinoso, F., Rouquerol, J., Sing, K.S.W., 2015. Physisorption of gases, with special reference to the evaluation of surface area and pore size distribution (IUPAC Technical Report). Pure Appl. Chem. 87 (9–10), 1051–1069.

Tian, Z., Li, H., Wei, Q., Qin, W., Yang, C., 2021. Effects of redox potential on chalcopyrite leaching: An overview. Miner. Eng. 172, 107135. https://doi.org/10.1016/j.mineng.2021.107135.

Wang, S., 2005. Copper leaching from chalcopyrite concentrates. JOM 57 (7), 48–51. https://doi.org/10.1007/s11837-005-0252-5.

Watling, H.R., 2013. Chalcopyrite hydrometallurgy at atmospheric pressure: 1. Review of acidic sulfate, sulfate–chloride and sulfate–nitrate process options. Hydrometallurgy 140, 163–180. https://doi.org/10.1016/j.hydromet.2013.09.013.

Yuan, Y., Bolan, N., Prévoteau, A., Vithanage, M., Biswas, K.J., Sik Ok, Y., Wang, H., 2017. Applications of biochar in redox-mediated reactions. Bioresour. Technol. 246, 271–281. https://doi.org/10.1016/j.biortech.2017.06.154.